Multimodal Neuroimaging based Alzheimer's Disease Diagnosis using Evolutionary RVFL Classifier

Tripti Goel*, *Member, IEEE*, Rahul Sharma, *Student Member, IEEE*, M. Tanveer*, *Senior Member, IEEE*, P. N. Suganthan* *Fellow, IEEE*, Krishanu Maji, Raveendra Pilli, Alzheimer's Disease Neuroimaging Initiative

***Abstract*—Alzheimer's disease (AD) is one of the most known causes of dementia which can be characterized by continuous deterioration in the cognitive skills of elderly people. It is a non-reversible disorder that can only be cured if detected early, which is known as mild cognitive impairment (MCI). The most common biomarkers to diagnose AD are structural atrophy and accumulation of plaques and tangles, which can be detected using magnetic resonance imaging (MRI) and positron emission tomography (PET) scans. Therefore, the present paper proposes wavelet transform-based multimodality fusion of MRI and PET scans to incorporate structural and metabolic information for the early detection of this life-taking neurodegenerative disease. Further, the deep learning model, ResNet-50, extracts the fused images' features. The random vector functional link (RVFL) with only one hidden layer is used to classify the extracted features. The weights and biases of the original RVFL network are being optimized by using an evolutionary algorithm to get optimum accuracy. All the experiments and comparisons are performed over the publicly available Alzheimer's Disease Neuroimaging Initiative (ADNI) dataset to demonstrate the suggested algorithm's efficacy.**

***Index Terms*—Alzheimer's Disease (AD), Magnetic Resonance Imaging (MRI), Positron emission tomography (PET), Random Vector Functional Link (RVFL), ResNet-50**

I. Introduction

Alzheimer's disease (AD) is one of the most prevalent and rapidly progressing neurological disorders among seniors. AD reveals the symptoms of dementia as it ages. Approximately 11,422,692 people (over 65 years aged persons) are agonizing from dementia only in India, according to the 2022 dementia report [9]. Aforesaid brain disease progresses with annihilating memory, thinking ability, and even the ability to accomplish quotidian chores. The aforementioned progressive malady permeates neurofibrillary tangles and amyloid plaques which are conceded neuropathological indicatory symptoms for AD. Considering extracellular dumping of amyloid-beta protein in deep grey matter generates the misfolded proteins formed in neuron cells which are known as amyloid plaques.

Neurofibrillary tangles originate from tau protein due to several anomalous chemical changes. Aforesaid plaques and tangles tort the neurons and catalyze disruption of the neural network system. Destruction of the connection between the neurons and the dying of the brain cells is the gradual manifestation of AD. Hitherto, there has been no remedy for this malady. The prognosis of AD at the preliminary phase is the only method that can do some prevention or may decelerate the health crisis worldwide. Currently, neuroimaging analysis has become rampant for the detection of AD. Neuroimaging techniques are a clinical non-invasive process that generates brain images to analyze abnormalities.

Amid neuroimaging techniques, PET and MRI scans are well known for AD detection. The PET imaging technique is one nuclear medicine paradigm for visualizing metabolic changes occurring at the cellular level in any organ or tissue. This technique injects radioactive tracers (drugs) to measure molecular activity within the specific ROI. 18F 2-Fluoro-2-deoxy-D-glucose (FDG) is a well-admitted tracing element in this approach. PET monitoring of cerebral glucose metabolism or amyloid deposition may provide an accurate diagnosis in the early stages of cognitive impairment. Multi-tracer PET scans help to understand the underlying pathological disease processes in Alzheimer's and the relationship between such abnormalities and patients' cognitive impairment. MRI uses magnetic resonance to create an image of the human body. In AD patients, the volume of the ventricles changes as compared to a healthy person's brain. Other structural changes in AD patients' brains include the decreased volumetric density of grey matter, impairment of the white matter, and changes in the hippocampus and cortical cortex. The structural and metabolic changes in cognitive normal (CN), mild cognitive impairment (MCI), and AD patients are shown in Fig. 1.

It is beneficial to use the fusion of more than one modality to enhance the accuracy and an extensive idea for the prognosis of AD. MRI and PET fused images will help to detect structural and metabolic abnormalities related to AD. Therefore, nowadays, multimodal data fusion of AD is a much more encouraging research field. This paper proposes the wavelet transform (WT)-based fusion model to fuse MRI and PET scans due to its multi-resolution handling process. The multimodal fusion technique may give better prediction than a single modal system in AD diagnosis.

Tripti Goel, Rahul Sharma, Krishanu Maji and Raveendra Pilli, Biomedical Imaging Lab, National Institute of Technology Silchar, Assam 788010, India (e-mail: triptigoel@ece.nits.ac.in, rahul_rs@ece.nits.ac.in, raveendra431@gmail.com, and krishanumaji_pg_21@ece.nits.ac.in)

M. Tanveer, Department of Mathematics, Indian Institute of Technology Indore, Simrol, Indore, 453552, India (e-mail: mtanveer@iiti.ac.in)

P. N. Suganthan, KINDI Center for Computing Research, College of Engineering, Qatar University, Doha, Qatar 2713, and also with the School of Electrical and Electronic Engineering, Nanyang Technological University, Singapore 639798 (e-mail: p.n.suganthan@qu.edu.qa)

Data used in this article were obtained from the Alzheimer's Disease Neuroimaging Initiative (ADNI) database (www.loni.ucla.edu/ADNI).

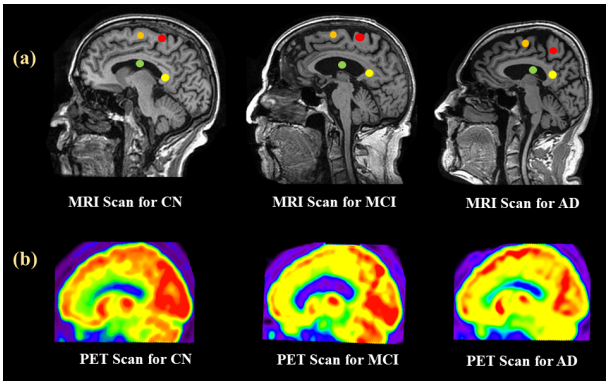

Fig. 1: a) Structural changes using MRI imaging, GREEN Dot denotes the volumetric change of ventricles, YELLOW dot denotes the change in the hippocampus region, ORANGE marked denotes changes in white matter, RED denotes the structural change of grey matter b) Metabolic changes using PET imaging

Over the last decade, machine learning (ML) techniques turned into the prime approach to lend a hand to researchers from predicting disease to drug delivery systems in biomedical science and acquiring intense understanding in deciphering obscure problems [10], [30]. Deep learning (DL) is the most promising subset of ML algorithms for the automatic feature extraction, feature reduction, and classification of images [16], [31]. Ganaie et al. [7] reviewed the recent works in ensemble DL along with the theoretical background and its applications in healthcare. Tanveer et al. [29] also implemented a deep model along with an ensemble approach for in-depth analysis of ROI-based features from MRI scans. Tanveer et al. [28] systematically reviewed the applications of DL for brain age estimation using neuroimages. In the present work, ResNet-50 [11], the DL model is used for the feature extraction from the fused images. ResNet-50 extracts high-rich features from the input images, and these features improve the DL model performance in classifying images.

The random vector functional link (RVFL) is a single hidden layer feedforward network (SLFN) in which the features from the hidden layer and the original input features are given to the output layer. During the training phase, the biases and weights of the hidden layer are randomly initialized within the desired range and remain constant during testing [19], [32]. The random initialization of weights and biases can result in non-optimal solutions. Therefore, this paper introduces a novel optimized RVFL network using a genetic algorithm (GA) to optimize the weights and biases of the RVFL network.

This study proposes a multimodal fusion-based DL network with an optimized RVFL model for AD diagnosis. This model is fed with T1-weighted MRI and PET scan data. The few significant contributions to this suggested work are listed below.

- In this paper, WT-based multimodal fusion is proposed to assimilate the structural and metabolite information to get ample information for AD prognosis.
- Staunch process of registration, image realignment, co-registration, and fusion of two different modalities (MRI and PET) employing appealing approaches, which will pave the way for multimodal fusion to provide additional information for diagnosis and prognosis.
- Optimal Selection of random parameter for RVFL using an evolutionary optimization algorithm.
- Fuzzy-based activation is used as an activation function for optimized RVFL.

The rest of the paper is organized as follows: Section II discusses the recent works on AD diagnosis. Section III represents the proposed methodology for AD diagnosis. Section IV presents the findings and opinions from this paper's corresponding analysis. Section V illustrates the conclusion and future scope of the work.

II. Related works

AD is a degenerative disorder that affects elderly people. It impairs one's cognitive function, making it difficult to do everyday business. A primary diagnostic tool in the fight against AD is now neuroimaging, thanks to fast advances in the field. Neuroimaging methods such as MRI and PET are commonly utilized to monitor the atrophies in brain tissue, both structural and metabolic. Regarding medical imaging, experts have looked at mixing various modalities rather than just one to get the most information. Gao et al. [8] presented a task-induced pyramid and attention generative adversarial networks (GAN) as a DL architecture to combine an image generation and AD classification task. An extra discriminator network is designed for classification, which increases the computational load. Qui et al. [20] fused MRI data along with neuropsychological testing, demographic information, and the medical background of the subjects in the evaluation process. The existence of neuropathological lesions on autopsy correlates strongly with disease-specific patterns discovered in the study, which demonstrates using interpretability approaches in computer vision. However, other multimodal neuroimaging data are not considered. Another multimodal approach incorporating four neuroimaging data is proposed in [34]. Feature fusion has been done, and classification has been made using multiclass SVM. However, the model is computationally much expensive.

Many multimodal fusion approaches incorporate feature concatenation. However, in [17], authors devised a method for AD detection and named it relation-induced multi-modal shared representation learning using regularization and relation-induced constriction. Abdelaziz et al. [1] implemented another multimodal fusion model by fusing MRI, PET, and genetic features extracted from different deep models. The model also performed regression tasks along with classification. However, the model accessed the ROI-based feature as input in this study.

Besides the multimodal approach, feature extraction is yet another challenge. Various state-of-the-art DL approaches perform exceptionally in high-level feature extraction. Feature extraction from the ResNet-50-based model is viral and has been adopted by various researchers [22], [23]. Zhang et al. [33] proposed a DL-based model with an attention module

for improved feature extraction using grey matter slice as input. However, the ROI-based input restricts the ability to understand much about the disease.

Recently, randomized networks have been widely adopted to obtain improved classification performance over traditional ML-based classifiers. RVFL and its variants have shown better performance over other randomized networks such as Extreme Learning Machine (ELM) [14]. Suganthan and Katuwal [25] discussed RVFL and its variants and evaluated the performance of RVFL through extensive comparisons over publicly available UCI datasets. Shi et al. [24] proposed an ensemble approach for RVFL by incorporating a stack of hidden layers. However, more hidden layers will increase the computational complexity of the model. In the proposed work, the weights and biases of the hidden layers of RVFL are optimized using evolutionary algorithms to achieve better accuracy for AD diagnosis. Cheng et al. [3] proposed another feature extraction method based on blocks-based residual networks. The approach proposed a diversified ensemble deep RVFL network by extracting the features from every block of 6-block ResNets and training the ensemble deep RVFL network. This methodology has higher computational complexity as a limitation of this paperwork. Huang et al. [13] extend ELM to Kernel ridge regression (KRR) which includes random hidden neurons and kernels to have better performance results with faster training speed. Ganaie et al. [6] proposed a novel ensemble deep RVFL network which incorporates privileged information along with standard information to get better generalization results.

In [31], authors perform spatial feature concatenation, which is extracted from different DL models, and then a comparison is made over several state-of-the-art classifiers. However, feature fusion over the frequency domain has not been performed. Another feature fusion approach in the frequency domain by performing slice fusion using WPT has been proposed in [5]. However, the model lacks multiclass classification, and a fuzzy-based SVM variant is incorporated, which leads to reduced performance for overlapping classes such as CN and MCI. Another approach that performs multiclass classification using feature fusion-based data has been proposed by Sharma et al. [21]. This paper incorporates five RVFL classifiers, and an ensemble of classifiers has been adopted for the classification approach, and the final decision has been made through majority voting. However, this approach is computationally expensive as it involves five RVFL classifiers to generate predictions.

According to findings, MRI and PET scans work together to identify Alzheimer's disease. PET/MRI gives more information regarding the underlying anatomical and metabolic abnormalities associated with AD than single-model approaches, which are more limited in their scope. This work proposes a multimodal slice fusion performed in the frequency domain using WT. The fused slice is fed to ResNet-50 for feature extraction and evolutionary optimization-based RVFL network to perform multiclass classification. For AD diagnosis, root means square error (RMSE) is used as the fitness function of evolutionary RVFL to optimize the biases and weights of the hidden layer. The following section introduces the details of the proposed network architecture.

III. Methodology

This section discusses the database used in this study and the proposed methodology, which includes preprocessing, feature extraction, and evolutionary algorithm-based RVFL classifier.

A. Dataset

For experiments and comparisons to diagnose AD, the data has been acquired from the Alzheimer's Disease Neuroimaging Initiative (ADNI) database. The principal purpose of ADNI was to follow the progression of MCI and early AD by employing longitudinal MRI, PET, other biological markers, and clinical and neuropsychological assessments. ADNI is divided into four stages, each with a distinct set of objectives and cognitive processes. The dataset includes subjects with cognitive normal (CN), mild cognitive impairment (MCI), and Alzheimer's disease (AD). T1-weighted MRI and 18F-FDG-PET scan images from the ADNI-1 database are utilized for training and evaluating our developed framework for each individual. 1.5 T scanners (SIEMENS maker) with 1.2mm slice thickness and 160 slices are used to obtain MRI scans. The dimension of each MRI scan is $256\times256\times166$. PET scans are captured using 1.5 T scanners (SIEMENS manufacturer) with a slice thickness of 2.4 mm. Each PET scan has a dimension of $160 \times 160 \times 93$. 210 CN, 210 MCI, and 210 AD subjects are selected for experiments. Fig. 4 shows the block diagram of the proposed model for AD diagnosis.

B. Preprocessing

The preprocessing of neuroimages is critical in illness diagnosis because it identifies missing important values, anomalies, and noise, including defects and outliers. These mistakes would remain if preprocessing were not done correctly, lowering the quality of model learning. Because MRI and PET scan capture distinct pieces of information, Co-registration between the two modalities is crucial for efficient fusion. Other preprocessing procedures include the elimination of undesired distortions and the amplification of specific image characteristics. Prior to image registration, both MRI and PET undergo Image Realignment and Image Normalization to regularize the intra-modal information. For assessments and additional processing, preprocessed images are appropriate. The complete pipeline of MRI and PET scan preprocessing is shown in Fig. 2. The following are the preprocessing steps:

- Inter-Modal Image Co-Registration: The comprehensive prognostic model for AD categorization may use MRI & PET scans from any available source. Every scanner has distinct scanning settings, including slice number, voxel size, etc. The 3D MRI and PET scans are coregistered via geometric modifications to make one scan fit into another. MATLAB SPM12 toolbox executes an affine registration with the $MNI-152$ template. The proposed work uses B-spline interpolation in the sixth order, with an average separation of $2mm \times 2mm$, and a Gaussian histogram smoothing in the seventh order. The registration is performed using normalized mutual information as

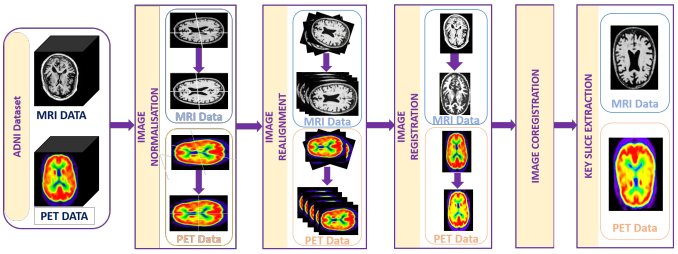

Fig. 2: Pipeline for preprocessing of MRI and PET scans

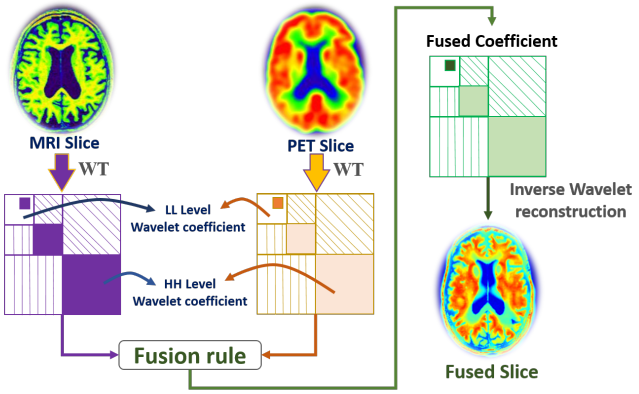

Fig. 3: Wavelet-based slice fusion of MRI and PET images

the goal function. All scans maintained the dimensions of $256 \times 256 \times 166$ after co-registration.

- Key Slice Extraction: Processing the whole 3D brain scan is computationally demanding and time-consuming. Key slice selection is performed to circumvent the limitations of 3D scan handling and render with more precision. The Grey Level Co-Occurrence Matrix (GLCM) derives statistical texture characteristics that best characterize the image's information. The proposed model extracts substantial slices using entropy and energy-based characteristics. These features tend to have low values in areas where diversity is strong and high values in areas where diversity is low. Because the atrophy-affected slices have low feature values, k-means clustering is employed to select meaningful slices according to differences in texture feature information.
- Slice fusion: Wavelet-based fusion approach is taken into account for the proposed approach, which is motivated by the previous work [5]. It is possible to combine images of various resolutions using wavelet-based fusion, which is a multiscale (multiresolution) approach. Although PET scans have lower spatial resolution than MRI images, the wavelet-based approach produces an unparalleled high-resolution image with metabolic and anatomical complexity. The discrete wavelet transform (DWT) separates the images into different coefficients. A combination of these coefficients yields new coefficients. Over the newly combined coefficients, an inverse discrete wavelet transform (IDWT) is applied.
  This 1D wavelet analysis can be extended to 2D by generating 2D wavelets and scaling functions as the tensor product of their 1D counterparts. $I_{LL}(x, y)$ is the coarse approximation of the image $I(x, y)$. $I_{LH}(x, y)$, $I_{HL}(x, y)$, and $I_{HH}(x, y)$ emphasize the horizontal, vertical, and diagonal aspects of picture I(x, y) (x, y). This study uses the Daubechies (db) 1 wavelet with level 4 decomposition. The db wavelet-based coefficients can accurately depict any frequency changes in a neuroscan. Coefficients acquired from MRI and PET scans are averaged before being merged. Fig. 3 visualizes the slice fusion approach for the proposed model.

C. Feature Extraction

DL is an enormous specialization of ML models. DL is suited for complicated tasks because of its ability to represent features at a deeper level by using numerous hidden layers. Layers of convolution and pooling are stacked to form the deep neural network (DNN). In the proposed methodology, ResNet-50 [11], a residual DNN with 50 layers, is used to derive new features that will be input to a classifier. Increasing the network's depth may enhance its accuracy and increase the likelihood of overfitting. As the network's depth increases, two issues arise vanishing gradient and degradation problem.

D. Evolutionary Algorithm based RVFL Classifier

1) RVFL: Due to the rise in the popularity of representational learning, randomized neural networks have also been growing in interest for classification. RVFL neural networks are preferable since they need less training time and provide good performance results. RVFL has a single hidden layer whose weights and biases are randomly initialized within the specified range. Weights and biases are fixed during the training phase; the closed-form solution calculates the output weights. RVFL generalization performance is boosted by direct linkages of the input features to the output layer, which is a regularization to improve the network's performance.

For arbitrary training data, $\{(x_{in}, t_{in})\}_{in=1}^{N}$, where $x_{in} \in R^d$ and $t_{in} \in R^c$, the input to the output layer of a RVFL consists of the output of hidden layer which is nonlinear generated features (denoted as H) and original features (denoted as X). The inputs to the output layer (D) are expressed by the formula $D = [H\ X]$. The total input features to the output layer may be expressed as $x_o = x_{in} + n$ where x_{in} is an input feature and n is the number of hidden neurons. The only parameter to be calculated during training is β, since the hidden layer has fixed weights w and biases b. Therefore, the resulting optimization problem of RVFL structure is expressed mathematically as

$$\min_{\beta} \parallel D\beta - O \parallel^2 + \lambda \parallel \beta \parallel^2 , \tag{1}$$

where λ represents the regularization parameter, and O represents the output target. β can be calculated using ridge regression (RR) or Moore–Penrose pseudo-inverse (MPPI). MPPI solution occurs when $\lambda = 0$ and output weights are calculated as $\beta = D^{+}O$. We incorporated both MPPI and RR in the proposed approach, and the model's performance is evaluated and tabulated.

At the hidden layer of the RVFL structure, the s-membership fuzzy function ($sFAF$) is introduced as the activation function. $sFAF$ transforms input features into the feature vector. The motivation for using $sFAF$ is to map outliers, either owing to motion artifacts or other reasons, to a range of zero or one membership value. For average levels of intensity, the outcomes are nearly linear. $sFAF$ is functionally expressed as:

$$\begin{aligned} A(i,k,m) =& 0, \qquad i \le k, \\ & 2^{f-1}\left(\frac{i-k}{m-k}\right)^f, \quad k < i \le \frac{(k+m)}{2}, \\ & 1-2^{f-1}\left(\frac{i-k}{m-k}\right)^f, \quad \frac{(k+m)}{2} < i < m, \\ & 1, \qquad i \ge m. \end{aligned} \tag{2}$$

Equation 2 is the functional expression of the $sFAF$. f monitors the slope of the $sFAF$ and is known as a fuzzifier. Two crossover points are presented by k, and m, at 0 as minima and 1 as maxima, respectively, along with the crossover point at $\frac{(k+m)}{2}$.

2) Evolutionary Algorithm-based Optimization: The hidden layer's weights and biases of the RVFL classifier are randomly initialized, and output weights are analytically calculated using MPPI and RR. The random initialization of weights and biases may give a non-optimal solution; therefore, this paper proposes an evolutionary algorithm-based optimization of input weights and biases and MPPI and RR to calculate the output weights. The genetic algorithm (GA) [4] is often used as a prominent optimization approach to solve global optimization problems. GA optimizes the network input parameters using root mean square error (RMSE) as the fitness function.

The following stages outline the evolutionary algorithm-based optimized RVFL method. In RVFL, the features extracted from the DL network are given as the input having n hidden nodes with an activation function $A(.)$.

- Initialization: The populations of the first generation, $\Theta_{l,G}$, is initiated with a set of NP vectors, each of which contains all of the network hidden node parameters.

$$\Theta_{l,G} = \left[a^T_{1,(l,G)}, ..., a^T_{H,(l,G)}, b_{1,(l,G)}, ..., b_{H,(l,G)}\right] \tag{3}$$

  where a_z and b_z are random generation with $z = 1, 2, ..., n$, G represents the generation and $l = 1, 2, ..., NP$.

- Calculation of fitness function: The fitness function will be calculated for each individual by taking RMSE as the cost function from the equations respectively.

$$RMSE_{l,G} = \sqrt{\frac{\sum_{in=1}^{N}\left\|\sum_{z=1}^{n}\beta_z A\left(a_{z,(l,G)}, b_{z,(l,G)}, x_{in}\right) - t_{in}\right\|}{c \times N}} \tag{4}$$

  The output of the hidden layer, $H_{l,G}$ can be represented as

$$H_{l,G} = \begin{bmatrix} A\left(a_{1,(l,G)}, b_{1,(l,G)}, x_1\right) & ... & A\left(a_{n,(l,G)}, b_{n,(l,G)}, x_1\right) \\ \vdots & \ddots & \vdots \\ A\left(a_{1,(l,G)}, b_{1,(l,G)}, x_N\right) & ... & A\left(a_{n,(l,G)}, b_{n,(l,G)}, x_N\right) \end{bmatrix} \tag{5}$$

  After the first generation, the best population vectors are stored, and D is calculated as $[H_{l,G}\ X]$.

- Crossover and Mutation: After initialization, evolutionary algorithms calculate the difference vector between the randomly generated population vector and the current existing population vector and generate the mutant vector. After generating the mutant vector, the crossover is performed following the crossover rate to control the fraction of the mutant vector copied to the next level.

- Selection: For selection, the difference between the fitness function of the current population and the crossover population is calculated. The solution that gives the fitness function's minimum value will be selected for the next generation, as demonstrated in equation (6)

$$\theta_{l,G+1} = \begin{cases} u_{l,G+1}, & if RMSE_{j(l,G)} - RMSE_{u_{(l,G+1)}} > \epsilon . RMSE_{j(l,G)}, \\ u_{l,G+1}, & if RMSE_{j(l,G)} - RMSE_{u_{(l,G+1)}} < \epsilon . RMSE_{j(l,G)} \\ & and \left\|\beta_{u_{(l,G+1)}}\right\| < \left\|\beta_{\theta_{(l,G)}}\right\|, \\ \theta_{l,G}, & else. \end{cases} \tag{6}$$

  Equation 6 is used to assess all trial vectors. $u_{l,G+1}$ is created at the crossover step, and ϵ is the predefined small positive tolerance rate.

Overall, a ResNet-50-based deep model assembles all levels of features from the fused multimodal scans. Later, the extracted feature is fed to the optimized RVFL network, and classification is made for the prognosis of AD. The impending section evaluates the proposed approach over different models and discusses the obtained performance metrics.

IV. Results and Discussion

This section illustrates the experimental results and state-of-the-art comparisons of the proposed evolutionary RVFL classifier using multi modal neuroimages.

A. Implementation details

The experiments are performed on a system with MATLAB R2021a, Intel(R) Core(TM) i7 − 8700 CPU @ 3.20GHz, 16-GB RAM, and a Windows-10 operating system. The ADNI dataset, including structural MRI and PET images, is used in all experiments. The dataset samples are randomly divided into 70 : 30 training and testing ratios. A total of 1000 preprocessed significant slices have been taken as input for the DL model. For the ResNet-50-based DL model, the following hyperparameter values have been considered to experiment. The minibatch size is 16, the learning rate at 0.01, $sgdm$ is the optimizer applied, and the epoch at 10 has been considered. The ResNet-50 is fed with fused slices to extract the features. Classification has been done over the extracted features for which evolutionary optimization-based RVFL has been incorporated with the hidden neuron values of 1000. All the network comparison and evaluation has been performed over the same mentioned hyperparameter.

This article has been accepted for publication in IEEE Journal of Biomedical and Health Informatics. This is the author's version which has not been fully edited and content may change prior to final publication. Citation information: DOI 10.1109/JBHI.2023.3242354

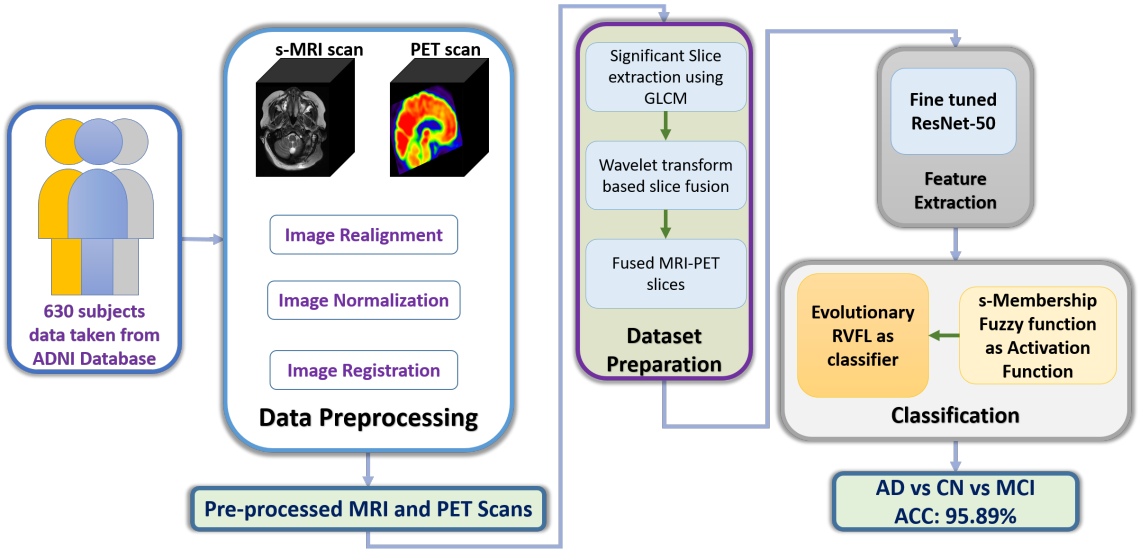

Fig. 4: Architecture of the proposed Evolutionary RVFL model

B. Experiment

The accuracy, sensitivity, specificity, precision, confusion matrix, and receiver operating characteristic (ROC) of the researched model are calculated for experiments. Specificity assesses the classifier's ability to identify disease-free individuals reliably. Sensitivity measures the classifier's ability to diagnose the person with the disease correctly. Precision measures the ratio of true diseased out of predicted diseased subjects. Accuracy can be elaborate as the authentic revealer of the entire process. Confusion matrices (CM) and ROC curves are graphical representations to predict the outcome of the process. CM shows the prediction analysis and helps to calculate the performance metrics necessary to deduce the conclusion. The ROC curves are sensitivity vs. specificity 2D plots. The curves near the left corner of the top will achieve good results.

C. Computational Complexity and Model Parameter Sensitivity Analysis

The proposed algorithm's computational complexity (CC) combines the CC of WT, DNN, and RVFL. To compute DWT for M points, the CC is $O(Mlog_2M)$. Training a ResNet-50 has a CC of $O(W^2s^2tLF)$, where W is the dimension of the fused images, s is the kernel size, t is the temporal dimensions, L is the total number of layers and F is the number of filters used. In RVFL networks, matrix inversion is used to determine the output weights. The dimensions of the input training data define the computation required for calculating the pseudo inverse. The computations required to calculate the output for RVFL of $N \times N$ matrix size is $O((N)^3)$. In the proposed optimized RVFL model, we used an evolutionary-based optimization algorithm. The CC of the optimization algorithm will be $O(Gnl)$, where G is the number of generations, n represents individual size and l represents population size.

In the proposed model, the randomly generated weights and biases of the RVFL network are optimized using GA. Therefore, model parameter sensitivity depends only on the number of hidden neurons, n. As shown in Table V, the results vary marginally due to the variation in the n; hence the proposed model does not have any parameter uncertainty.

D. Comparison with different modalities

In this comparing inspection amid PET, MRI, and fusion-based imaging, ResNet-50 is implemented for every modality, and classification is done using evolutionary-RVFL. Table I shows the comparative results regarding accuracy, specificity, sensitivity, and precision. Figure 3 shows the comparison using the CM and ROC curves. As illustrated, the fusion-based classification ROC curve with the top-left corner proposes the usefulness of the fusion-based imaging data. As represented in table 1, the accuracy of the fused image is much higher and most favorable than MRI and PET imaging. The inadequacy of the single modality detection process can elucidate the inferior performance of MRI and PET scan images.

TABLE I: Evaluation of the proposed model's performance utilizing multiple modalities (in %)

Modality	Accuracy	Specificity	Sensitivity	Precision
MRI only	93.44	95.83	88.67	91.41
PET only	91	88.83	**95.33**	81.02
Fusion	**95.89**	**96.17**	**95.33**	**92.56**

E. Comparison with different DL networks

Several revolutionary DL representations differentiate the proposed ResNet-50-based DL technique in this subsection to demonstrate proficiency in AD prognosis. There are several DL methods to extract features like GoogleNet [26], DenseNet [12], Inceptionv3 [27], SqueezeNet [15], and ResNet-50 [11] which are being used to differentiate the outcomes. The features of pre-processed and fused data scans are extracted by different DL models individually and then extracted features are fed to the proposed evolutionary RVFL network. The

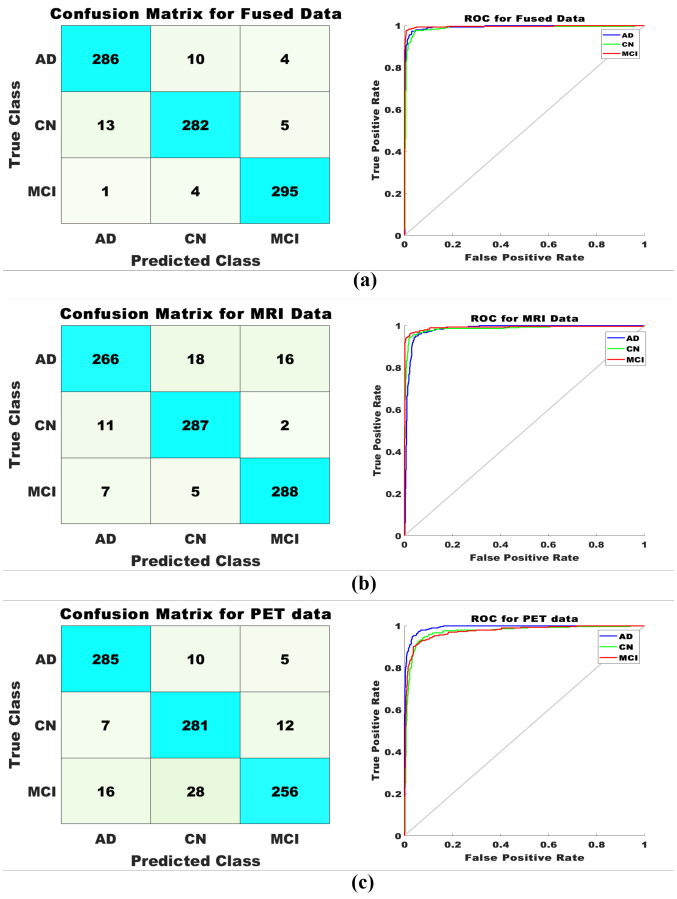

Fig. 5: Confusion Matrix and ROC of a) Fused dataset b) MRI dataset c) PET dataset

differentiation among the performance matrices of the DL network is condensed in Table II.

TABLE II: Comparison of the proposed model's performance with state-of-the-art DL architectures(in %) for CN vs AD vs MCI classification

Model	Accuracy	Specificity	Sensitivity	Precision
Inceptionv3 [27]	55.33	55.83	54.33	38.08
SqueezeNet [15]	72.56	71.50	74.67	56.71
GoogleNet [26]	86.56	86.17	87.33	75.94
DenseNet [12]	71.11	70.50	72.33	55.08
ResNet-50	**95.89**	**96.17**	**95.33**	**92.56**

F. Comparison with variants of RVFL and other randomized networks

In this subsection, RVFL variants that include dRVFL [24], edRVFL [24], ELM [14], KRR [13], random forest (RF) [2] followed by non-optimized standard RVFL [18] and the softmax classifier are evaluated and compared to demonstrate proficiency of the proposed model. Overall, the optimization helps in improving the classification accuracy of the model. The differentiation among the performance matrices of the compared models in terms of accuracy, sensitivity, specificity, and precision are tabulated in Table III.

TABLE III: Performance comparison of suggested model with state-of-the-art SLFN models (in %) for CN vs AD vs MCI classification

Model	Accuracy	Specificity	Sensitivity	Precision
Standard RVFL [18]	64.78	47.50	**99.33**	48.61
Softmax [11]	85.22	81.82	94.0	66.67
ELM [14]	57.89	48	77.67	42.75
KRR [13]	57.33	55	62	40.79
RF [2]	89.56	86.67	95.33	78.14
dRVFL [24]	86.22	92.33	80	83.92
edRVFL [24]	95.11	**96.50**	95.67	**93.18**
Proposed+MPPI	92.33	92.83	91.33	86.44
Proposed+RR	**95.89**	96.17	95.33	92.56

G. Comparison with different activation functions

In this subsection, fuzzy activation functions are compared with other traditional activation functions like sigmoid, sine, Triangular basis (TriBas), Hard Limit (HardLim), Rectified Linear Unit (ReLU), Scaled Exponential Linear Unit (SELU), and Radial Basis (RadBas). The comparison is shown in Table IV to show the significance of using the s-membership fuzzy activation function for the proposed evolutionary RVFL classifier. s-membership fuzzy activation function removes the outliers and maps the input vector into the range from zero to one membership value.

TABLE IV: Performance evaluation of the suggested model with various activation functions (in %) for CN vs AD vs MCI classification

Model	Accuracy	Specificity	Sensitivity	Precision
Sigmoid	86.33	88	83	77.57
Sine	87.22	88.83	84	79
TriBas	87.33	89	84	79.25
HardLim	87	88	85	77.98
RadBas	86.89	89.17	82.33	79.17
ReLU	87.11	87	87.33	77.06
SELU	87.22	88.50	84.67	78.64
s-Membership	**95.89**	**96.17**	**95.33**	**92.56**

H. Comparison with different numbers of neurons

RVFL classifier efficiency mainly depends on the count of neurons used in the hidden layer, with a trade-off with computational complexity. Table V shows the performance of the proposed model with the different numbers of neurons. 1000 number of neurons is the most optimal number of neurons with the highest performance obtained, and the performance varies marginally as we increase or decrease the number of neurons.

TABLE V: Comparison of the proposed model's performance with different numbers of hidden neurons(in %) for CN vs AD vs MCI classification

Model	Accuracy	Specificity	Sensitivity	Precision
100	95.78	96	95.33	92.26
200	95.33	95.50	95	91.35
300	95.67	95.33	**96.33**	91.17
500	95.56	95.67	95.33	91.67
700	95.78	96.17	95	92.53
1000	**95.89**	**96.17**	95.33	**92.56**
2000	95.44	95.50	95.33	91.37

Among the several techniques, we can confidently anticipate that the multi-modal Wavelet fusion-based ResNet-50 model will outperform the others.

I. Discussion

The suggested multi-modality fusion-based model in this research illustrates the efficiency of multimodality over a single modality for AD diagnosis. The high computational cost for 3D scans is also decreased in this study by adopting key slice extraction based on the GLCM feature extraction process without reducing the system's accuracy. In the Co-registration method, we are doing an inter-modality registration process, in which MRI and PET modalities have different resolutions due to two different scanners outcomes, without hampering the image quality. The co-registration process provides the most effective image for fusion. To justify this, we calculate the accuracy of the raw and preprocessed data. The slices of raw MRI and PET scans are fused together, and the proposed model with the RR approach has been used to determine the classification performance. An accuracy of $85.44,\%$ has been obtained, which is very less because raw scan slices vary from subject to subject; hence, the common brain region present in particular slices may not match with the other subject slice. Similarly, the importance of significant slice selection plays a vital role after preprocessing. We select a total of 5 significant slices from each MRI scan based on the entropy and energy-based characteristics. We evaluated the model performance over a single middle slice extracted from preprocessed scans to justify the slice selection significance. We obtained an accuracy of 89.56% over the proposed model with the RR approach, and the obtained performance is very low as compared to the performance obtained from training the model over significant slices.

The suggested model is evaluated over multimodality fused data and single modality data for diagnosing AD. It is shown that the multimodality fusion-based data give better results than the single modality. It is because single modality data can't provide the metabolic and structural data altogether. After several comparing surveys, it can be predicted that ResNet-50 can present a better outcome as a feature extractor among multiple numbers of DL techniques. State-of-the-art DL models are also compared in Table II for feature extraction. Table 2 shows the best performance results for ResNet-50 for feature extraction. For experiments, the proposed fuzzy activation function-based evolutionary RVFL classifier is used for fair comparisons.

For the classification of the features extracted from ResNet-50, the RVFL classifier is used further to improve the model's performance for AD diagnosis. As the weights and biases of RVFL classifiers are randomly assigned, evolutionary RVFL is proposed to improve accuracy. In Table III, the proposed variant of RVFL, evolutionary RVFL, is compared with the standard RVFL and other variants of RVFL, like edRVFL and dRVFL. Also, the proposed evolutionary RVFL is compared with the other randomized neural network, an extreme learning machine (ELM). To show the significance of using the s fuzzy activation function for RVFL, the comparison has been made with other standard activation functions in Table IV.

Different comparisons shown through Table I to Table V show that the proposed model based on multimodal fusion and fuzzy activation function-based evolutionary RVFL gives the best results as compared to state-of-the-art methods.

V. Conclusions and Future Works

In elderly people, Alzheimer's disease (AD) causes a nonreversible loss of cognitive abilities, making it one of the leading causes of death. When AD is diagnosed at the early stage of mild cognitive impairment (MCI), the clinicians have a better chance of converting the patient back to cognitive normal (CN) by prescribing the appropriate medication. Therefore, the proposed paper focuses on diagnosing AD effectively at the early stage using 210 AD, 210 MCI, and 210 CN subjects of MRI and PET scans. MRI and PET scans have different information and acquisition parameters, image registration and co-registration of these scans have been done using the standard MNI-152 template. In this paper, we fused MRI and PET scans using Wavelet Transform (WT) to obtain structural and metabolic information. The ResNet-50 network is used to extract the features of the fused images, and extracted optimal features are fed to the RVFL network for classification. To further improve performance, weights and biases of the RVFL classifier are optimized using an evolutionary algorithm. In the evolutionary RVFL structure, s fuzzy activation function maps the input vector into feature space.

The performance of the proposed model is evaluated by carrying out the experiments using single modality vs. multimodality, Standard RVFL and its variants, different DL models for feature extraction, and s fuzzy activation function compared with other activation functions. The proposed evolutionary RVFL model achieves the best overall results for CN vs. MCI vs. AD classification in terms of accuracy, specificity, sensitivity, and precision. The main limitation of the present study is to consider only structural and metabolic changes in AD patients. Further, in this study, we focused mainly on multiclass classification between CN vs MCI vs AD, ignore the prediction of MCI to AD.

Future work can be extended to include other modalities like: functional MRI, Susceptibility Weighted Images, diffusion tensor imaging, etc., for AD diagnosis. Further, other optimization variants, like swarm optimization, can be used to optimize the parameters of RVFL and the variants of RVFL.

Acknowledgment

This work is supported by the National Supercomputing Mission under DST and Miety, Government of India, under Grant No. DST/NSM/R&DHPCAppl/2021/03.29. This work is also supported by Core Research Grant to the Science and Engineering Research Board (SERB) for funding under Grant No. CRG/2022/006866.

References

[1] M. Abdelaziz, T. Wang, and A. Elazab, "Alzheimer's disease diagnosis framework from incomplete multimodal data using convolutional neural networks," *Journal of Biomedical Informatics*, vol. 121, p. 103863, 2021.

[2] L. Breiman, "Random forests," *Machine learning*, vol. 45, no. 1, pp. 5–32, 2001.

[3] W. X. Cheng, P. N. Suganthan, and R. Katuwal, "Time series classification using diversified ensemble deep random vector functional link and resnet features," *Applied Soft Computing*, p. 107826, 2021.

[4] S. Das, S. S. Mullick, and P. N. Suganthan, "Recent advances in differential evolution–an updated survey," *Swarm and evolutionary computation*, vol. 27, pp. 1–30, 2016.

[5] S. Dwivedi, T. Goel, M. Tanveer, R. Murugan, and R. Sharma, "Multimodal fusion based deep learning network for effective diagnosis of Alzheimers disease," *IEEE MultiMedia*, 2022.

[6] M. Ganaie and M. Tanveer, "Ensemble deep random vector functional link network using privileged information for Alzheimer's disease diagnosis," *IEEE/ACM Transactions on Computational Biology and Bioinformatics*, 2022.

[7] M. A. Ganaie, M. Hu *et al.*, "Ensemble deep learning: A review," *arXiv preprint arXiv:2104.02395*, 2021.

[8] X. Gao, F. Shi, D. Shen, and M. Liu, "Task-induced pyramid and attention gan for multimodal brain image imputation and classification in Alzheimers disease," *IEEE Journal of Biomedical and Health Informatics*, 2021.

[9] S. Gauthier, P. Rosa-Neto, J. Morais, and C. Webster, "World Alzheimer Report 2021: Journey through the diagnosis of dementia," *Alzheimer's Disease International*, 2021.

[10] S. Grueso and R. Viejo-Sobera, "Machine learning methods for predicting progression from mild cognitive impairment to Alzheimer's disease dementia: a systematic review," *Alzheimer's Research & Therapy*, vol. 13, no. 1, pp. 1–29, 2021.

[11] K. He, X. Zhang, S. Ren, and J. Sun, "Deep residual learning for image recognition," in *Proceedings of the IEEE conference on computer vision and pattern recognition*, 2016, pp. 770–778.

[12] G. Huang, Z. Liu, L. Van Der Maaten, and K. Q. Weinberger, "Densely connected convolutional networks," in *Proceedings of the IEEE conference on computer vision and pattern recognition*, 2017, pp. 4700–4708.

[13] G.-B. Huang, H. Zhou, X. Ding, and R. Zhang, "Extreme learning machine for regression and multiclass classification," *IEEE Transactions on Systems, Man, and Cybernetics, Part B (Cybernetics)*, vol. 42, no. 2, pp. 513–529, 2011.

[14] G.-B. Huang, Q.-Y. Zhu, and C.-K. Siew, "Extreme learning machine: theory and applications," *Neurocomputing*, vol. 70, no. 1-3, pp. 489–501, 2006.

[15] F. N. Iandola, S. Han, M. W. Moskewicz, K. Ashraf, W. J. Dally, and K. Keutzer, "Squeezenet: Alexnet-level accuracy with 50x fewer parameters and $<$ 0.5 mb model size," *arXiv preprint arXiv:1602.07360*, 2016.

[16] A. Loddo, S. Buttau, and C. Di Ruberto, "Deep learning based pipelines for Alzheimer's disease diagnosis: a comparative study and a novel deep-ensemble method," *Computers in Biology and Medicine*, vol. 141, p. 105032, 2022.

[17] Z. Ning, Q. Xiao, Q. Feng, W. Chen, and Y. Zhang, "Relation-induced multi-modal shared representation learning for Alzheimer's disease diagnosis," *IEEE Transactions on Medical Imaging*, vol. 40, no. 6, pp. 1632–1645, 2021.

[18] Y.-H. Pao and Y. Takefuji, "Functional-link net computing: theory, system architecture, and functionalities," *Computer*, vol. 25, no. 5, pp. 76–79, 1992.

[19] Y.-H. Pao, G.-H. Park, and D. J. Sobajic, "Learning and generalization characteristics of the random vector functional-link net," *Neurocomputing*, vol. 6, no. 2, pp. 163–180, 1994.

[20] S. Qiu, M. I. Miller, P. S. Joshi, J. C. Lee, C. Xue, Y. Ni, Y. Wang, D. Anda-Duran, P. H. Hwang, J. A. Cramer *et al.*, "Multimodal deep learning for Alzheimer's disease dementia assessment," *Nature communications*, vol. 13, no. 1, pp. 1–17, 2022.

[21] R. Sharma, T. Goel, M. Tanveer, P. N. Suganthan, I. Razzak, and R. Murugan, "Conv-ervfl: Convolutional neural network based ensemble rvfl classifier for alzheimer's disease diagnosis," *IEEE Journal of Biomedical and Health Informatics*, pp. 1–9, 2022.

[22] R. Sharma, T. Goel, M. Tanveer, S. Dwivedi, and R. Murugan, "FAF-DRVFL: Fuzzy activation function based deep random vector functional links network for early diagnosis of Alzheimer disease," *Applied Soft Computing*, vol. 106, p. 107371, 2021.

[23] R. Sharma, T. Goel, M. Tanveer, and R. Murugan, "FDN-ADNet: Fuzzy LS-TWSVM based deep learning network for prognosis of the Alzheimer's disease using the sagittal plane of MRI scans," *Applied Soft Computing*, vol. 115, p. 108099, 2022.

[24] Q. Shi, R. Katuwal, P. N. Suganthan, and M. Tanveer, "Random vector functional link neural network based ensemble deep learning," *Pattern Recognition*, vol. 117, p. 107978, 2021.

[25] P. N. Suganthan and R. Katuwal, "On the origins of randomization-based feedforward neural networks," *Applied Soft Computing*, vol. 105, p. 107239, 2021.

[26] C. Szegedy, W. Liu, Y. Jia, P. Sermanet, S. Reed, D. Anguelov, D. Erhan, V. Vanhoucke, and A. Rabinovich, "Going deeper with convolutions," in *Proceedings of the IEEE conference on computer vision and pattern recognition*, 2015, pp. 1–9.

[27] C. Szegedy, V. Vanhoucke, S. Ioffe, J. Shlens, and Z. Wojna, "Rethinking the inception architecture for computer vision," in *Proceedings of the IEEE conference on computer vision and pattern recognition*, 2016, pp. 2818–2826.

[28] M. Tanveer, M. Ganaie, I. Beheshti, T. Goel, N. Ahmad, K.-T. Lai, K. Huang, Y.-D. Zhang, J. Del Ser, and C.-T. Lin, "Deep learning for brain age estimation: A systematic review," *arXiv preprint arXiv:2212.03868*, 2022.

[29] M. Tanveer, A. H. Rashid, M. Ganaie, M. Reza, I. Razzak, and K.-L. Hua, "Classification of Alzheimer's disease using ensemble of deep neural networks trained through transfer learning," *IEEE Journal of Biomedical and Health Informatics*, vol. 26, no. 4, pp. 1453–1463, 2021.

[30] M. Tanveer, B. Richhariya, R. U. Khan, A. H. Rashid, P. Khanna, M. Prasad, and C. Lin, "Machine learning techniques for the diagnosis of Alzheimer's disease: A review," *ACM Transactions on Multimedia Computing, Communications, and Applications (TOMM)*, vol. 16, no. 1s, pp. 1–35, 2020.

[31] J. Venugopalan, L. Tong, H. R. Hassanzadeh, and M. D. Wang, "Multimodal deep learning models for early detection of alzheimer's disease stage," *Scientific reports*, vol. 11, no. 1, pp. 1–13, 2021.

[32] L. Zhang and P. N. Suganthan, "A comprehensive evaluation of random vector functional link networks," *Information sciences*, vol. 367, pp. 1094–1105, 2016.

[33] Y. Zhang, Q. Teng, Y. Liu, Y. Liu, and X. He, "Diagnosis of Alzheimer's disease based on regional attention with sMRI gray matter slices," *Journal of neuroscience methods*, vol. 365, p. 109376, 2022.

[34] Y. Zhang, S. Wang, K. Xia, Y. Jiang, P. Qian, and A. D. N. Initiative, "Alzheimer's disease multiclass diagnosis via multimodal neuroimaging embedding feature selection and fusion," *Information Fusion*, vol. 66, pp. 170–183, 2021.